# Review of Interpretation Method of Global Strain Measurement in Pile Testing

Liew, S.S.[1], Lim, Jason A.H.[2] and Chin, Y.L.[3]

*[1,2 and 3]G&P Geotechnics Sdn Bhd, 39-5, Jalan Tasik Selatan 3, Kuala Lumpur 57000, Malaysia*
*E-mail*: ssliew@gnpgroup.com.my

**ABSTRACT:** This paper aims to present a new theoretical framework relating the global elastic strain measurement of discrete pile segments with strain-dependent pile stiffness modulus to the pile-soil load transfer profiles. With the measured pile elastic deformation of each pile segment from global strain gauges, there are always seven possible scenarios of shaft friction profile with either upward or downward directions varying with depth of either increasing or decreasing trend or maintaining constant along the pile segment that can permissibly yield the same elastic shortening as measured. Hence the relationship of pile elastic deformation with respect to the interpreted pile shaft resistance profile is not unique. Because of uncertainties in the assumed pile shaft profile during the planning of the test pile instrumented segments, remarkable flaws in back inference of the pile load transfer mechanism from global strain measurement is possible. The larger the instrumented pile segment length, the more uncertainties and potential flaws there will be. Illustration of these seven scenarios will be presented to reveal these potential impacts. Two methods of interpreting the pile axial load profile will be discussed in this paper. The first method is mid-segment pile axial load method as conventionally adopted by most pile testing specialists due to its simplicity and robustness of calculation and second method is pile segment end-point reactions method, which is more sensitive to numerical instability. However, the numerical instability can conveniently prompt the possible wrong assumption in adopting one out of the seven scenarios as mentioned.

Another important aspect of pile lock-in strain resulting from pile installation process or unloading load cycle during load testing can have effect to the subsequent measured global strain in the pile segment. Despite being practically difficult to account for such disturbing factor, knowing the effect may help to improve the understanding of certain pile behavioural trends, like stiffening pile load-settlement in reloading cycles and inter-transfer of reducing downward pile shaft friction to incremental pile test load. This paper will present and discuss this effect.

**KEYWORDS:** Global Elastic Strain, Strain-dependent Stiffness, Shaft Friction, End Bearing, Lock-in Stress/Strain, Hysteresis

## 1. INTRODUCTION

Pile instrumentation is a very popular topic attracting many geotechnical engineers in debating about the testing methods, procedures and interpretation as it provides the performance data determining the success or failure of a pile foundation in terms of capacity and deformation. There is a relationship linking these two engineering behaviours with the load transfer mechanism between the pile body and the embedding soils. In most foundation applications, action is imposed onto the pile body with resisting reaction derived from supporting soils. Occasionally there can be a situation where the pile element behaves as a resisting element to the deforming soil media against the foundation pile, for instance, downdrag action onto the pile embedded in a compressing or consolidating soil body embedding a pile.

With the structural stress-strain behaviour of the pile body, one can measure the change of axial strain of pile section, then interpret the philosophical stress within the pile section to deduce the axial forces at both ends of pile segment to understand how the load transfer mechanism behaves with the pile segment. A pile instrumentation scheme can be implemented by measuring either localised strain and global strain within the pile body to provide useful insights of load transfer performance of pile. There are several pile instrumentation schemes which include weldable vibrating wire strain gauges (Dunnicliff, 1988), removal extensometers (Bustamante *et at*., 1991, Faisal *et al*., 2008 and Krishnan *et al*., 2006) and fibre optic strain sensors (Glisic *et al*., 2002).

## 2. THEORETICAL FRAMEWORK

### 2.1 Non-Linearity of Concrete Elasticity

It is well-known that the elasticity of concrete material does not remain constant over the range of stressing history during loading and unloading cycles, but rather exhibiting a strain softening behaviour with increasing stress level. From many strain measurements at the calibrating segment with strain gauges immediately below the load imposition at pile top with no external forces interfering the pile axial load within the calibrating segment, the back-calculated secant Young Modulus can be approximately represented by a linear regression function as shown in Figure 1, where $E(z)$: Secant Young Modulus of Concrete; $\varepsilon(z)$: Measured Local Compressive Strain or

Average Global Compressive Strain; m: Negative Constant for Reduction Rate of Secant Young Modulus; $E_0$: Initial Tangential Young Modulus at Zero Concrete Strain; z: Location of the Infinitesimal Pile Segment. The accuracy of the pile stiffness modulus is very sensitive to the pile elastic shortening, in which underprediction can yield excessive pile shortening, thus giving unrealistically high pile axial load at the adjoining pile segment, vice versa. The hysteresis between the loading and unloading cycles presents different stiffness response over the same stressing/straining range of piles. However, it is necessary to have the conventional regressed line of the pile stiffness modulus as initial values to derive the pile axial stress. The regressed pile stiffness modulus used in the case study of this paper is presented in Figure 1.
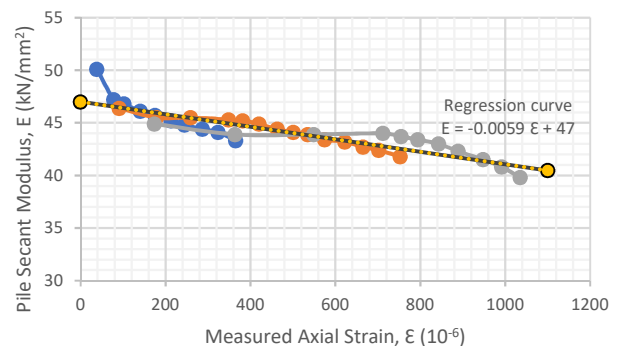


Figure 1 Strain-Dependant Pile Secant Stiffness Modulus with Axial Strain

### 2.2 Load Transfer and Elasticity Models of Pile Segment

For simplicity, Figure 2 illustrates a simple schematic model with three external loads exerting to the pile segment, namely $P_T$: Top axial load of pile segment; F: Pile shaft resistance of pile segment; $P_B$: Bottom axial load of pile segment, whereas L: Length of pile segment; $\delta$: Elastic shortening of pile segment; z: Location of interested physical quantity from top of pile segment.

The middle schematic diagram of Figure 2 presents the linearly distributed profile of mobilised shearing stress along the pile shaft surface where $f_{s,T}$ is shearing stress at top of pile segment and $f_{s,B}$ is

shearing stress at bottom of pile segment. The rightmost schematic diagram of Figure 2 shows the pile axial load profile along the entire pile segment, in which C is pile circumference.
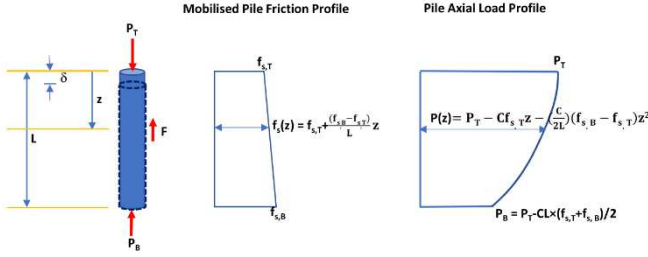


Figure 2 Load Transfer and Elastic Deformation Model of Pile Segment

### 2.3 Derivation of Pile Segment Shortening from Profile of Pile Shaft Resistance

Based on simple elasticity theory, substituting pile secant modulus, $E(z) = m\varepsilon(z) + E_0$, in Figure 1 and pile axial load, $P(z)$, in Figure 2 into the elasticity formulae in Eq. (1), where A is pile sectional area,

$$\varepsilon(z) = \frac{\sigma}{E(z)} = \frac{\frac{P(z)}{A}}{m\varepsilon(z) + E_0} \tag{1}$$

$$\Leftrightarrow \varepsilon(z)A = \frac{P(z)}{m\varepsilon(z) + E_0} = \frac{P_T - Cf_{s,T}Z - \frac{C}{2L}(f_{s,B} - f_{s,T})Z^2}{m\varepsilon(z) + E_0}$$

$$\Leftrightarrow Am\varepsilon(z)^2 + AE_0\varepsilon(z) - [P_T - Cf_{s,T}Z - \frac{C}{2L}(f_{s,B} - f_{s,T})Z^2] = 0$$

Solving the above quadratic equation for the roots of $\varepsilon(z)$, where $a = Am \neq 0$, $b = AE_0$, $c = -[P_T - Cf_{s,T}Z - \frac{C}{2L}(f_{s,B} - f_{s,T})Z^2]$

$$\Rightarrow \varepsilon(z) = \frac{-b \pm \sqrt{(b^2 - 4ac)}}{2a} = \frac{-AE_0 \pm \sqrt{[(AE_0)^2 - 4Am(Cf_{s,T}Z + \frac{C}{2L}(f_{s,B} - f_{s,T})Z^2 - P_T)]}}{2Am}$$

$$= -\frac{E_0}{2m} \pm \sqrt{[(\frac{E_0}{2m})^2 - \frac{Cf_{s,T}Z + \frac{C}{2L}(f_{s,B} - f_{s,T})Z^2 - P_T}{Am}]}$$

As one of the root yields extremely high elastic strain with corresponding very low secant Young modulus of pile, thus the only valid root with negative constant, m, to yield sensible positive value of $\varepsilon(z)$ shall be as follow:

$$\varepsilon(z) = -\frac{E_0}{2m} - \sqrt{[(\frac{E_0}{2m})^2 - \frac{Cf_{s,T}Z + \frac{C}{2L}(f_{s,B} - f_{s,T})Z^2 - P_T}{Am}]}$$
$$= k - \sqrt{[k^2 - hz - gz^2 + p]} \tag{2}$$

where $k = -\frac{E_0}{2m}$; $g = -\frac{C(f_{s,B} - f_{s,T})}{2ALm}$; $h = -\frac{Cf_{s,T}}{Am}$; $p = \frac{P_T}{Am}$

The elastic shortening, $\delta$, of the pile segment length of L can be determined by integrating Eq. (2) to yield Eq. (3), (4) and (5) with the corresponding trend of pile shaft friction profiles.

For increasing pile shaft friction profile ($g = -\frac{C(f_{s,B} - f_{s,T})}{2ALm} > 0$), where $q = \sqrt{\frac{(gp + gk^2 - \frac{h^2}{4})}{g^2}}$;

$$\delta = \int_0^L \epsilon(z)dz = \int_0^L \{k - \sqrt{[k^2 + hz + gz^2 + p]}\}dz$$
$$= kL - \sqrt{g} \int_0^L \sqrt{[(Z + \frac{h}{2g})^2 + q^2]}dz$$
$$= kL - \frac{\sqrt{g}}{2}\{(L + \frac{h}{2g})\sqrt{[(L + \frac{h}{2g})^2 + q^2]} + q^2 \ln \left|(L + \frac{h}{2g}) + \sqrt{[(L + \frac{h}{2g})^2 + q^2]}\right| - (\frac{h}{2g})\sqrt{[(\frac{h}{2g})^2 + q^2]} - q^2 \ln \left|(\frac{h}{2g}) + \sqrt{[(\frac{h}{2g})^2 + q^2]}\right|\} \tag{3}$$

For decreasing pile shaft friction profile ($g = -\frac{C(f_{s,B} - f_{s,T})}{2ALm} < 0$), where $q = \sqrt{\frac{(|g|p + |g|k^2 + \frac{h^2}{4})}{g^2}}$;

$$\delta = \int_0^L \epsilon(z)dz = \int_0^L \{k - \sqrt{[k^2 + p + hz - |g|z^2]}\}dz$$
$$= kL - \sqrt{|g|} \int_0^L \sqrt{[(\frac{k^2 + p}{|g|}) + \frac{h^2}{4g^2} - (z - \frac{h}{2|g|})^2]}dz$$
$$= kL - \frac{\sqrt{|g|}}{2}\{(L - \frac{h}{2|g|})\sqrt{[q^2 - (L - \frac{h}{2|g|})^2]} +$$
$$q^2 \tan^{-1} \frac{(L - \frac{h}{2|g|})}{\sqrt{[q^2 - (L - \frac{h}{2|g|})^2]}} - (\frac{-h}{2|g|})\sqrt{[q^2 - (\frac{h}{2|g|})^2]} -$$
$$q^2 \tan^{-1} \frac{-\frac{h}{2|g|}}{\sqrt{[q^2 - (-\frac{h}{2|g|})^2]}}\} \tag{4}$$

For constant pile shaft friction profile ($g = -\frac{C(f_{s,B} - f_{s,T})}{2ALm} = 0$), where $q = -\frac{(k^2 + p)}{h}$;

$$\delta = \int_0^L \epsilon(z)dz = \int_0^L \{k - \sqrt{[k^2 + hz + p]}\}dz$$
$$= kL - \sqrt{h} \int_0^L \sqrt{[z - q]}dz$$
$$= kL - \frac{2\sqrt{h}}{3}[(L - q)^{\frac{3}{2}} - (-q)^{\frac{3}{2}}] \tag{5}$$

From the derivation of Eq. (1) to (3), the elastic shortening of pile segment by integrating the strain profile of the pile segment is equivalent to the area of the strain profile over the pile segment length. As such, when the pile shaft friction profile is constant across the pile segment, the pile strain profile shall be an approximately linearly increasing relationship if the non-linearity of the pile secant modulus is negligible and also the pile segment length is short. The average strain equivalent to the integrated area of the linear strain profile will be the mean value lying very close to the mid-point of the linearly increasing strain profile. However, if the pile shaft friction profile is not constant, but rather is either linearly increasing or decreasing, then the average value of pile axial strain will not be at the mid-point of the actual non-linear strain profile depending of the shape of the strain profile of either concave or convex curve respectively. If the non-linearity of the pile secant modulus is collectively considered, higher degree of non-linearity can be expected in the pile axial strain profile resulting further deviation of the location of average strain value from the mid-point. This is because of higher degree of non-linearity as evidenced in Eq. (1). When the pile axial load is higher with corresponding lower pile secant modulus, the pile axial strain will comparatively increase, whereas lower pile axial load with corresponding higher pile secant modulus, the pile axial strain will be lower, thus increasing the curvature of the pile axial strain profile and so as its degree of non-linearity. It will be interesting to note that the general cases of the shearing stress distribution profile with the boundary values of $f_{s,T}$ and $f_{s,B}$ at both ends of pile segment, which can be either zero (without side shearing stress), constant with either upwards (positive friction) or downwards (negative friction) stresses, and linearly increasing or decreasing side shearing stress with either upwards (positive friction) or downwards (negative friction) direction as shown in Figure 3. There are possibly seven different conditions of shearing stress distribution for a given measured global strain over the pile segment, thus the inference of shearing stress profile from global strain measurement is not necessarily unique. Therefore, assumption of shearing profile and their shearing direction along the pile shaft shall be carefully assessed from the available subsurface investigation information and then decided for the appropriate interpretation of the global strain instrumentation results. This paper will further focus on pile load test cases with only compressive test load and positive mobilized side friction (upward direction) of either constant, linearly increasing or decreasing trends.
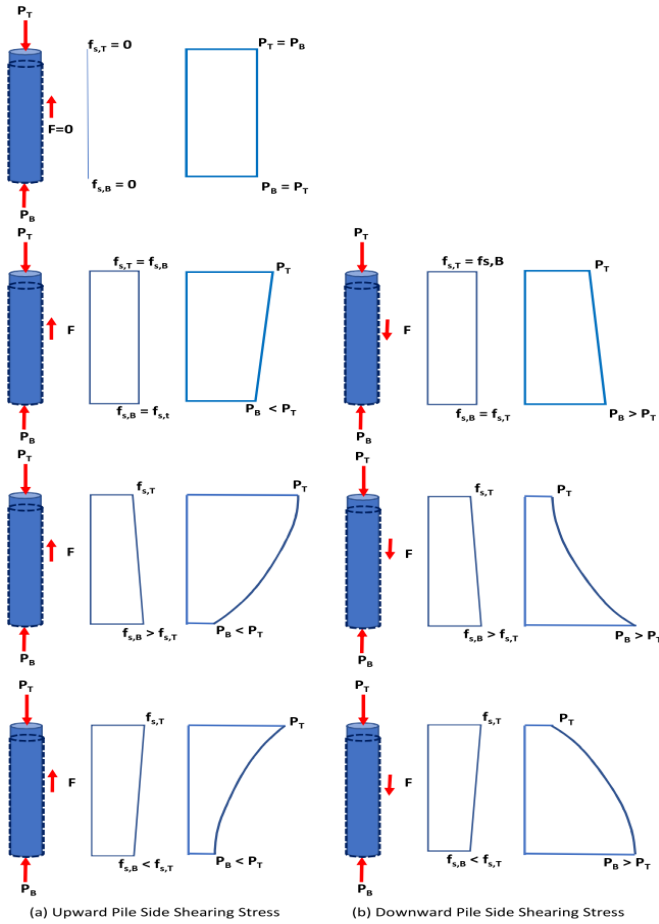
(a) Upward Pile Side Shearing Stress    (b) Downward Pile Side Shearing Stress

Figure 3 Mobilised Pile Shaft Friction Profiles with corresponding Pile Axial Load Profile along Pile Shaft

## 2.4 Present Interpretation Approaches of Global Strain Measurement and The Problems

Presently the widely accepted mid-segment pile axial load method has been the most popular approach due to its robustness and good numerical stability of the interpreted results. This method derives the pile axial load from the measured global strain of instrumented pile segment between the global strain extensometer anchoring points with correction to non-linearity concrete secant Young modulus and the interpreted axial compressive load is assumed at the middle of each instrumented pile segment. With the pile axial load profile established from the average compressive strain using global strain measurement, the mobilised pile shaft friction is derived from the incremental change of interpreted pile axial load and their averaged movement at the mid-point of each pile segment for the load transfer relationship. However, this method has inherently assumed constant pile shaft friction between the mid-points of each pile segment. As a result, this method has inherent problems if the nodal points of instrumented pile segments do not coincide well with the expected interface of subsoil strata and the significant contrast in material strength and stiffness. In addition, the effect of overly averaging in the global strain with huge contrast within excessively long instrumented pile segment, where there are noticeable important subdivisions of engineering soil stratification for necessary demarcation of separate pile shaft friction profile, can yield significantly erroneous and unrepresentative interpretative outcomes. On the other hands, the averaging effect in this method has made the results very robust and numerically stable in processing the global strain measurement data even with some unavoidable typical instrumentation error in the global strain measurement between the extensometer anchoring points.

This paper explores another interpretation approach considering the elastic shortening measured between the anchoring points of global strain extensometer at both ends of the pile segment, in which

the node points of the interpreted pile axial load coincide exactly at the extensometer anchoring points. The data processing procedures are summarized as follows:

a. The pile axial load imposition at top of test pile shall be taken as a starting axial load with expected attenuation of pile axial load along the back-calculated pile shaft friction of corresponding pile segments from the measurement of global strain extensometer as mentioned in Item (b) below.

b. With the appropriately assumed profile of pile side shearing stress ($f_{s,T}$ and $f_{s,B}$ at both ends of pile segment), pile circumference (C) and the pile segment length (L) and the top segment load ($P_T$), iteration of the assumed gradient profile of $f_{s,T}$ and $f_{s,B}$ values can be performed to obtain approximate elastic shortening from the integrated global strain as from Eq. (3), (4) or (5), whichever shaft friction profile is appropriate, and match the measured shortening of pile segment.

c. The interpreted mobilized pile shaft friction along the whole pile segment can be deduced from deduction of the bottom load ($P_B$) of pile segment from the top segment load ($P_T$) over the pile shaft surface area of the pile segment.

d. Take the computed bottom load from upper pile segment as the top load for the next pile segment and repeat Steps (a) to (c) for the bottom load of each pile segment.

e. With the absolute nodal movement by cumulating the pile top movement measurement and the measured shortening of global strain measurement for each pile segment, the load transfer relationship of pile shaft friction with corresponding mobilized pile nodal movement (at mid-point of pile segment) can then be established.

The only drawback of this end-point method is its lack of robustness in numerical stability if there is noticeable measurement error in the global strain measurement and any error in the parameters used in deriving the global strain of pile segment as discussed in Section 3. Figure 4 shows the comparison of the two approaches in deriving the pile axial load and its assigned location.
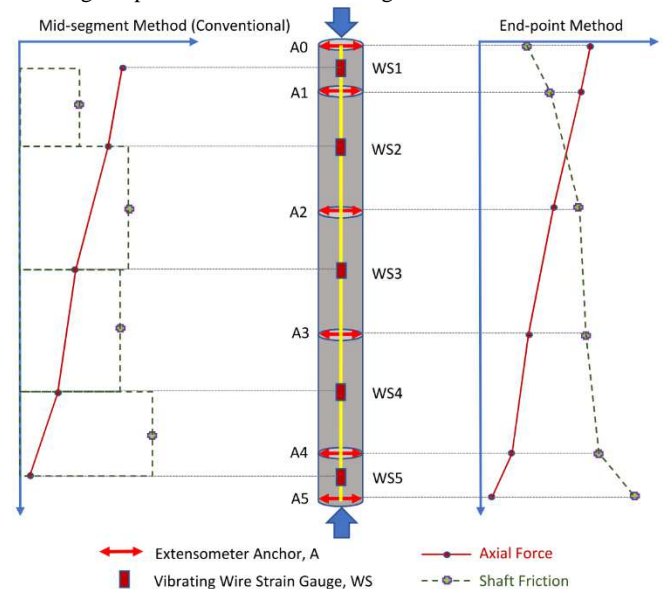


Figure 4 Comparison of Interpretation Methods of Global Strain Measurement in Pile Load Test

The major differences are that the new end-point reaction method derives all the pile axial forces at the pile nodal points, which is also the physical boundary of the individual instrumented pile segment. The derived pile shaft friction is distributed along the individual pile segments, in which the trend of shaft friction distribution profile can be assigned with the end values of $f_{s,T}$ and $f_{s,B}$ at both end of the pile segment depending on the actual subsurface conditions. In fact, the mid-segment method is a special case of the end-point method under the scenario of constant shaft friction profile.

## 3. DISCUSSIONS ON COMPARISON OF APPROACHES

In this section, comparison of two idealistic scenarios between the new computation framework and the conventional approach will be discussed. Both cases presented here have considered the same behavior of strain dependent secant modulus of pile stiffness.

The first scenario (Case A) is based on the computed elastic shortening (taken as measured global strain of eight pile segments with total pile segment length of 39.5m) derived from a given profile of pile axial load with a fictitious profile of pile shaft friction, thus ideally having no measurement error whereas the second scenario (Case B) is based on the actual measured data set repeating the same data processing procedures of the two approaches to demonstrate the difference of outcome due to the probable measurement error in pile shortening and also accuracy of pile stiffness modulus. In addition, it is believed that the difference is also dependent to the degree of discretization of the instrumentation pile segment length with respect to the sensitivity in variation of actual pile shaft friction profile within the pile shaft segment.

In Case A, the interpreted pile axial load profile between the two approaches are identical and perfectly match the initial shaft friction profile used to generate the elastic shortening of the corresponding pile segments. The mid-segment method produces the pile axial load at mid-point of each pile segment, which is derived from the average strain of the global strain shortening between the two ends of each pile segment in the end-point method. However, it is mathematically curtailed that if the pile friction profile is not constant along the pile segment, then the pile axial load in the mid-segment method still deviates from the end-point method as the linearly varying pile friction profile will have the pile axial load profile in quadratic curve, not a linear line, especially for the condition of very long instrumented pile segment and also severely varying in pile shaft friction profile. Another observation is that the pile axial load profile in the end-point method has all the axial loads at the end points of each pile segment matched continuously without any discrete values at the adjoining pile segments. Figure 5 shows the outcome of the interpretation of the two fictitious data set of opposite trends in pile shaft friction profiles, in which the increasing trend produces a concave profile pile axial load (upper diagram) whereas the reducing trend produces a convex profile (lower diagram). The interpreted profile of pile axial load using the mid-segment method and end-point method shows good match between the two. The only difference is that the pile axial load from the mid-segment method (blue circular dots) lies approximately at the average value of the pile axial loads (red rhomboid dots) at both ends of the corresponding pile segment. If combining the second to seventh pile segments as one longer instrumented pile segment of 37.5m, the interpreted pile axial load located at the mid-point of the long pile segment is denoted as the green triangular symbol in Figure 5. It is evidenced that the pile axial loads in both shaft friction profiles interpreted from the mid-segment method do not coincide with the corresponding pile axial profiles as elaborated in earlier section in this paper.

In Case B with assuming constant shaft friction profile, it is obvious that the measurement error in the end-point method has resulted in overprediction of the bottom axial load from the uppermost pile segment probably due to slightly underestimated pile secant modulus in Figure 1. Once the deviation of pile axial load is derived for the top load of the next lower pile segment, the next bottom load will swing to opposite direction for matching the computed pile segment shortening. In particular, the lowest short pile segment yielding nearly local strain for good estimation of pile end bearing load, whereas the end-point reaction method produces very unrealistic profile and end bearing load. The phenomenon indicates an oscillation of alternatingly over and under prediction with larger variation as the propagating error keeps compounding the magnitude of error as in Figure 6. It is believed that the assumed constant shaft friction pile in this assessment might not be an appropriate assumption. Conversely, the mid-segment method robustly produces a relatively smooth and apparently logical pile axial load profile. However, there exists doubt on the accurate representation of the pile

axial load profile and the appropriateness of the pile shaft friction profile assumed as evidenced earlier. From the soil consistency profile in borehole information, it is also anticipated that the friction profile at seventh and eighth pile segments shall have same friction, thus the pile axial profiles at the two pile segments shall have the same gradient. But there are obviously two different gradients in these two pile segments, it is certainly valid to suspect the interpreted pile axial profiles might need further refinement for sensible outcome.

If iteration by adjusting the measured global strain of pile segments from top down can be performed to attain a smoothen profile of interpreted pile axial load, then the measurement error can be back inferred and quantified with some confident level.
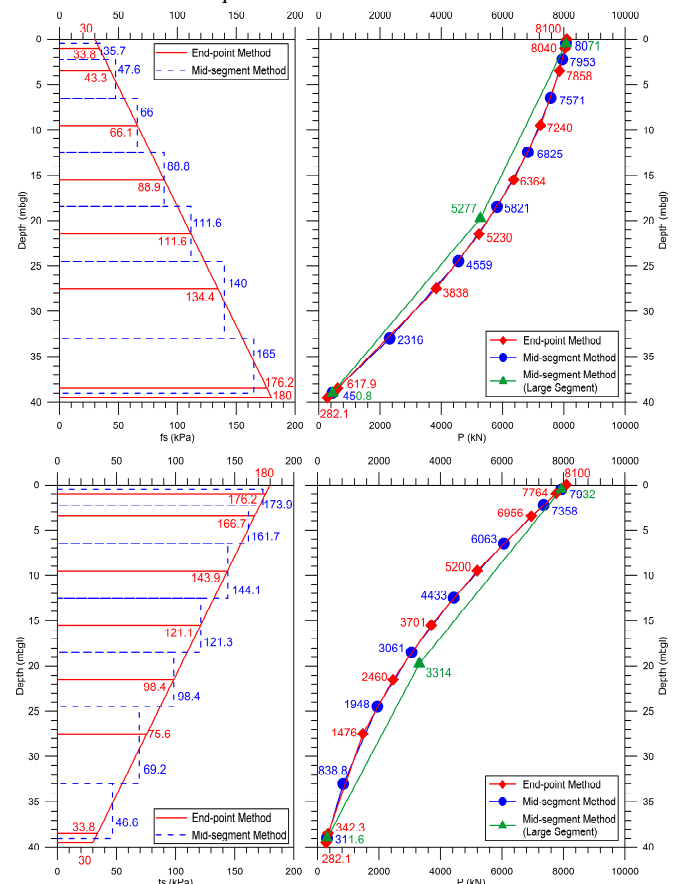


Figure 5 Comparison of Interpretation Methods of Global Strain Measurement in Pile Load Test with Ideally Fictitious Data Sets of Increasing and Reducing Trend of Pile Shaft Friction Profile
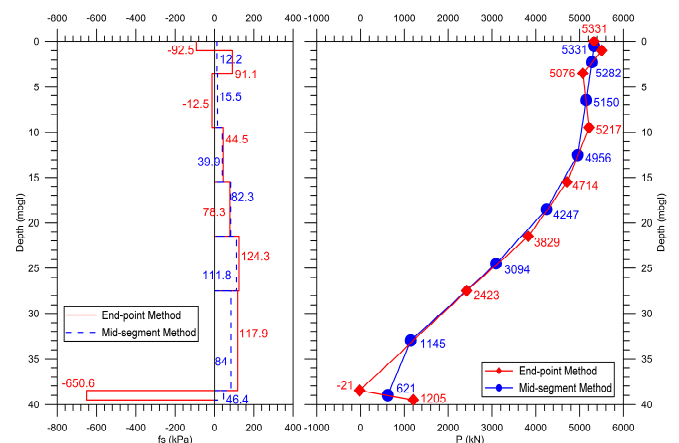


Figure 6 Two Interpretation Methods on Actual Global Strain Instrumentation Data

In planning of pile instrumentation scheme, it is vital to identify the subsoil stratification, which provides the information on appropriate trend of shaft resistance profile. Hence, having the pile

nodal points for interpreted pile axial load located at the interfaces between different soil strata will allow appropriate interpretation of limiting pile shaft resistance of the respective strata. The new proposed pile segment end-point reactions method will have advantage in this instance. For the conventional mid-segment method, there exists a possibility of smearing the resistances from two adjoining soil strata across the global strain measurement segment resulting in potential unrepresentative pile axial load interpretation. As for an accurate pile end bearing measurement, it is not difficult to understand that the best way is to have the global strain with very short gauge length for determination of nearly local strain for accurately interpreted pile axial load immediately above the pile toe.

## 4. LOCK-IN STRESS EFFECTS, NON-LINEARITY & HYSTERESIS OF PILE-SOIL INTERFACE ELASTO-PLASTIC BEHAVIOUR

Pile with repeated unloading and reloading cycles normally performs with much stiffer load settlement performance from observing the load-settlement results, which can be explained with the probable lock-in axial compressive stress in the pile after unloading. The installed pile is initially subject to compressive load during pile installation operation until attaining both the ultimate pile shaft and toe resistances with pile-soil interface slippage for pile penetration to target length or capacity. However, upon unloading, the elastic rebound of the initially compressed pile will subject to downdrag load where the pile-soil resistance will have to act in the reverse direction at the upper portion of pile. As a result, the initially compressed pile cannot have a full recovery of the earlier elastic compressive straining, then the lock-in compressive stress exists within the pile as schematically shown in Figure 7. This phenomenon of lock-in stress is equivalent to prestressing the pile before loading the pile with actual service load. The overall load-settlement behaviour of the pile with lock-in stress shall be much stiffer as shown in Figure 8 because the gradually imposing service load to the pile will take over the downdrag without further straining the pile. Liew & Ho (2016) and Liew (2017) have discussed some aspects of the phenomenon of lock-in stress during pile installation. The impacts of lock-in stress to strain measurement are the initial stress level in the pile existed before the pile instrumentation with the subsequent incremental loading process and, also the correct pile secant modulus to be used without the strain level ascertained.

From observing most pile load settlement results, behavioural models of bi-linear, tri-linear or even non-linear hyperbolic function have been postulated for simulating the recoverable elastic and non-recoverable plastic behaviour of overall pile response under loading at macroscopic level. Some even put remarkable efforts in examining the localised load transfer of a series of discretised pile segments with interfaces to soils at microscopic scale. Generally non-linear elastic behaviour is sparsely observed in geotechnical materials. When stress-strain relation exhibits non-linearity, it is mostly contributed from the unrecoverable plastic deformation at the pile-soil interface or the supporting soil itself.

Elastic behaviours of pile and embedding soil shall result in all deformations within the pile-soil interface system to be fully recoverable with no residual deformation after completely unloaded. If there is observed unrecoverable plastic deformation, the deformation mostly comes from either slippage at the pile-soil interface or localised yielding or particle dislocation of the embedding soil with local shear stresses beyond the soil strength or both. Once the plastic deformation occurs, creeping behaviour under sustained loading of adequate magnitude causing localised yielding when the redistribution of the stress field to reach new equilibrium and hysteresis phenomenon can be observed in statically cyclic loading process. The elasticity of the loaded materials and load path in dispersing the load imposition from the supporting pile to foundation soils, there will be different degree of stress mobilisation in the load dispersing process, particularly with a relatively large stress field system. Some are well under stressed, some at state of yielding, and some are stressed beyond the strength. The non-linearity

of stress-strain behaviour is a gross summation of the different degree of stress mobilisation with unrecoverable plastic deformation. In both the forwarding and reversal of stressing process, localised yielding and slippage at pile-soil interface resulting to partial plastic deformation with energy loss during the loading or unloading process, thus increasing the non-linearity. It is such non-linearity causing the separation of the stress-strain paths in energy injection and energy recovery of the system.
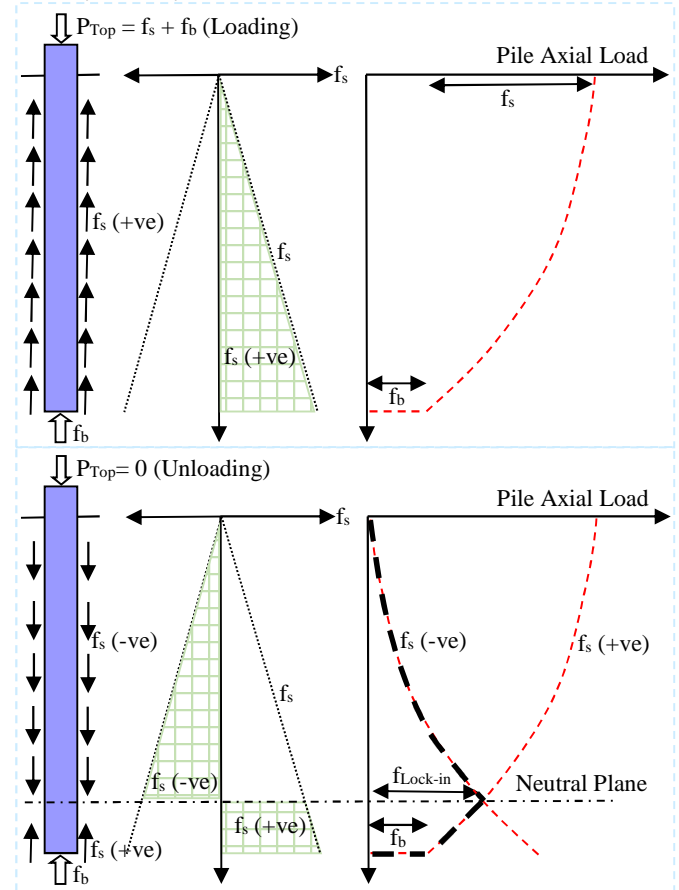


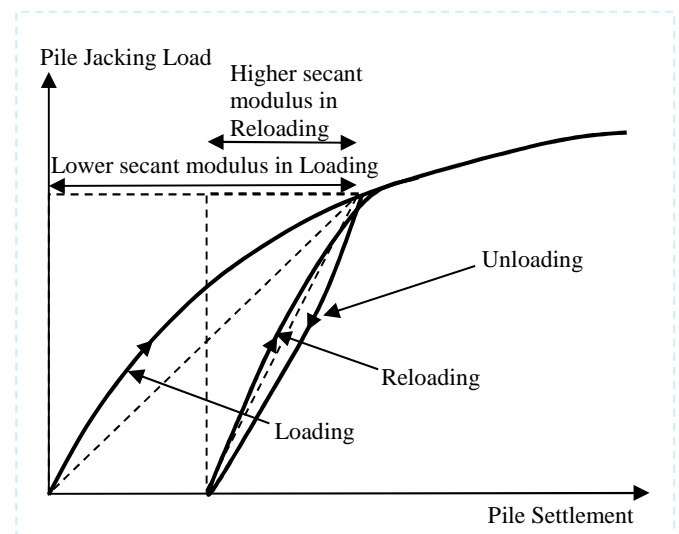Figure 7 Effect of Lock-in Stress in the Loading and Unloading Cycles in a Jack-in Pile



Figure 8 Pile Stiffening Effect in the Loading and Unloading Cycles of a Jack-in Pile with Lock-in Stress

Figure 9 shows a typical load settlement curve of static maintained load test results. The portion from Point 1 to 2 denotes linear elastic behaviour when there is no part of the pile-soil system attaining either interface slippage and dislocation of soil grains. Full

recovery of elastic strain of pile structure and foundation soil is possible with this range of loading. However, when the pile loading passes beyond Point 2, either soil yielding or interface slippage at the upper portion of the pile-soil system occur. The lower pile segments may remain in elastic behaviour. When the loading is stressed beyond Point 3, more yielding of soil and interface slippage occur and extend to lower pile segments resulting more irrecoverable straining. Upon reaching the first maximum test load at Point 4 following with unloading process to Point 5 and subsequently to Point 6, partial restoration of the stored elastic strain energy in the pile-soil system takes place.

When the restoration of elastic strain between the pile and the soil becomes inconsistent due to either soil grain dislocation or interface slippage, the reaction at the upper pile segments can be in a reverse direction, hence preventing full release of the elastic strain in the piles becoming the lock-in load in the pile. As illustrated in Figure 7, the static equilibrium of the pile-soil system at this state is attained with downward drag force at the upper pile segment and upward resistances from the lower pile segment and pile toe. Maximum compressive load is located at the neutral plane where the downward and upward resistances meet. When the test pile is reloaded again, normally the initial stiffer response at the beginning of reloading can usually be observed when comparing to the earlier loading cycle. This is primarily due to much lower elastic shortening ($\delta_{top}$ - $\delta_{NP}$) with relatively high pile stiffness when reloading of the pile by taking over the downward drag load in the soil above the neutral plane to reach static equilibrium. It can be logically expected that the pile deformation, $\delta_{NP}$, at the neutral plane when first attained in the loading cycle shall remain unchanged in the unloading and reloading cycle as the upward resistance is the same for these three loading cycles.

It will be interesting to examine the possible pile stiffening response when such lock-in load exists in the pile due to installation process and, also preloading before pile testing. In jack-in pile system, such effect is more prominent than driven pile as static jacking can preserve better lock-in load in pile comparing to dynamic percussion piling method. For cast-in-situ bored pile, such lock-in load may only momentarily exist during the volumetric expansion due to thermal hydration. After cooling down, even tensile load can exist in the pile if not slight compressive load.

Due to the high creep potential when the stress-strain behaviour of a pile subject to loading with remarkable plastic deformation in embedding soil and slippage at the pile-soil interface, it is suggested to observe the sustainable stabilised pile loading as the test load where the initial high rate of creeping settlement attenuates to attain the static equilibrium. For instance, when the pile is loaded reaching the aforementioned state, the recorded loading onto the pile will reduce from the last incremental test load to a slightly lower, but stable load reaching the static equilibrium.
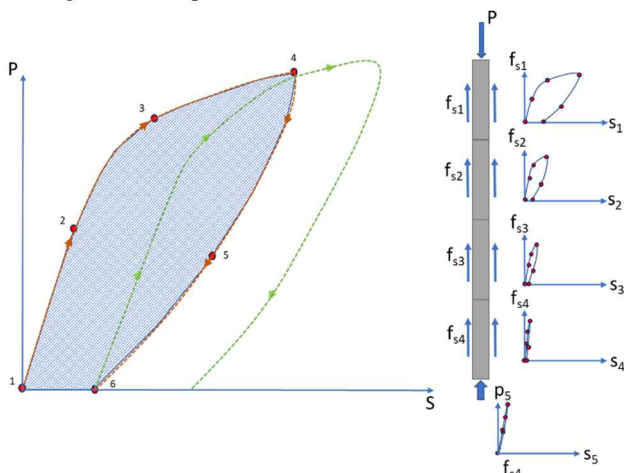


Figure 9 Schematic Diagram of Pile Load Test Results

## 5. CONCLUSIONS AND RECOMMENDATIONS

This paper has presented a new interpretative approach of global strain measurement with varying pile secant stiffness modulus under rigorous closed-form solution framework, namely pile segment end-point reactions method, in pile load test instrumentation. The following findings and conclusions can be summarised:

a. The relationship between pile elastic deformation and pile shaft resistance is not unique as there are total seven possible profiles of pile shaft friction distribution with the same elastic shortening.

b. Comparisons between the two methods in both ideal case and actual instrumentation data have been performed and summarised to show the errors and the associated problems. The new method agrees perfectly with the ideal case and exhibits numerical instability when processing the actual instrumentation data set.

c. The conventional mid-segment method is a special case of the newly proposed end-point method in this paper by assuming constant friction within the instrumented pile segment. However, this conventional method is simple, robust and not subject to numerical instability, thus can readily yield results with apparently logical and smooth profile of pile axial load.

d. Severe interpretative error in the global strain measurement can happen if the instrumented pile segment is overly long and there is drastic variation of the pile shaft friction profile due to different soil strata within the instrumented pile segment.

e. If the pile shaft friction profile is not constant, then compounding error propagating along the pile shaft segments will deviate the actual value in the conventional mid-segment method.

f. For pile end bearing capacity, it is best to have the global strain with very short gauge length approximating to local strain to interpret pile axial load immediately above the pile toe as the end bearing load.

g. The mechanism of lock-in stresses in pile installation and pile load test has been discussed in detail and also highlighted its impacts on determining initial pile axial profile with lock-in stress and strain affecting the correct determination of pile secant modulus in the global strain measurement.

## 6. REFERENCES

Dunnicliff, J. (1988) "Geotechnical Instrumentation for Monitoring Field Performance". Wiley, New York, pp467-479.

Bustamante, M., and Doix, B. (1991) "A new model of LPC removable extensometer". Proceedings 4th International Deep Foundation Institute Conference, pp475-480.

Faisal, Hj. A., and Lee, S. K. (2008) "New Instrumentation Technique for Piles". The International Conference on Advances in Civil Engineering, Cyprus, pp17-24.

Krishnan, S., and Lee, S. K. (2006) "A Novel Approach to the Performance Evaluation of Driven Prestressed Concrete Piles and Bored Cast-in-place Piles". Proceedings 10th International Conference on Piling and Deep Foundations, Amsterdam.

Glisic, B., Inaudi, D., and Nan, C. (2002) "Pile Monitoring with Fiber Optic Sensors during Axial Compression, Pullout and Flexure Tests". Transportation Research Record 1808, pp11-20.

Liew, S. S. and Ho, S. F. (2016) "Fallacy of Capacity Performance & Innovation Improvement of Jack-In Piling in Malaysia". Geotechnical Engineering Journal of the SEAGS & AGSSEA Vol. 47 No.1 March2016 ISSN 0046-5828

Liew. S.S., (2017) "Common Blind Spots in Ground Investigation, Design, Construction, Performance Monitoring and Feedbacks in Geotechnical Engineering", 50th Anniversary Symposium, Asian Institute of Technology, Bangkok, Thailand, 14-15 September 2017.